

Comparative first-principles calculations of the electronic, optical, elastic and thermodynamic properties of XCaF_3 ($X = \text{K}, \text{Rb}, \text{Cs}$) cubic perovskites



Li Li^{a, b}, Y.-J. Wang^{a, b}, D.-X. Liu^a, C.-G. Ma^a, M.G. Brik^{a, c, d, *}, A. Suchocki^{a, b, e}, M. Piasecki^d, A.H. Reshak^{f, g}

^a College of Mathematics and Physics, Chongqing University of Posts and Telecommunications, 2 Chongwen Road, Nan'an District, Chongqing 400065, PR China

^b Institute of Physics, Polish Academy of Sciences, Al. Lotników 32/46, 02-668 Warsaw, Poland

^c Institute of Physics, University of Tartu, W. Ostwald Str. 1, Tartu 50411, Estonia

^d Institute of Physics, Jan Długosz University, Armii Krajowej 13/15, PL-42200 Częstochowa, Poland

^e Institute of Physics, Kazimierz Wielki University, Weyssenhoffa 11, 85-072 Bydgoszcz, Poland

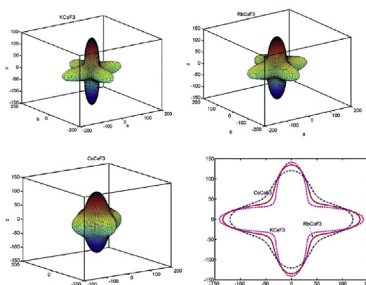
^f New Technologies – Research Centre, University of West Bohemia, Univerzitní 8, 306 14 Pilsen, Czechia

^g School of Material Engineering, University Malaysia Perlis, 01007 Kangar, Perlis, Malaysia

HIGHLIGHTS

- Three cubic perovskites XCaF_3 ($X = \text{K}, \text{Rb}, \text{Cs}$) were studied by ab initio methods.
- Systematic variation of physical properties with the first cation change was traced.
- Pressure effects on physical properties were calculated and modeled.
- Debye temperature and Grüneisen constant for all materials were calculated for the first time.
- Elastic anisotropy was visualized by plotting Young moduli directional dependences.

GRAPHICAL ABSTRACT



ARTICLE INFO

Article history:

Received 18 October 2016

Received in revised form

7 December 2016

Accepted 12 December 2016

Available online 18 December 2016

Keywords:

Perovskites

ab initio calculations

Electronic structure

Elastic and thermodynamic properties

ABSTRACT

Three fluoroperovskites with the general formula XCaF_3 ($X = \text{K}, \text{Rb}, \text{Cs}$) have been systematically studied using the first-principles methods. The structural, electronic, optical, elastic and thermodynamic properties of these three compounds were calculated at the ambient and elevated hydrostatic pressure. Variation of all these properties with pressure was analyzed; it was shown that the structural and elastic constants change linearly with increased pressure, whereas the calculated band gaps follow the quadratic dependence on pressure. Influence of the first cation variation ($\text{K} - \text{Rb} - \text{Cs}$) on these properties was discussed. Elastic anisotropy (directional dependence of the Young moduli) of these compounds was modeled and analyzed for the first time.

© 2016 Elsevier B.V. All rights reserved.

* Corresponding author. Institute of Physics, University of Tartu, W. Ostwald Str. 1, Tartu 50411, Estonia.

E-mail address: mikhail.brik@ut.ee (M.G. Brik).

1. Introduction

Chemical formula of crystals with cubic perovskite structure can be generally written as ABZ_3 , where A and B are the metal cations, and Z can be one of these elements: O, F, Cl, Br, I. They form a very large family of compounds [1–4], which are of high importance for numerous technological applications due to their diverse optical, electronic, electric, magnetic etc properties [5–9]. Many experimental and theoretical works, which investigate selected properties of some representatives of this group of materials, can be found in the literature. In the present paper we have chosen three cubic fluoroperovskites $XCaF_3$ ($X = K, Rb, Cs$) for the systematic first-principles calculations of their structural, electronic, optical, elastic and thermodynamic properties at ambient and elevated hydrostatic pressure.

Some properties of these compounds have been studied before, but never at such scale. For example, the change of the band gap character from indirect to direct when varying the first cation from K to Cs in these three perovskites was detected in Ref. [10]. The pressure effects on the elastic, electronic and optical properties of $KCaF_3$ were studied in Ref. [11] using the WIEN2K code. The $KCaF_3$ and $RbCaF_3$ perovskites were considered in Refs. [12,13], whereas the $KCaF_3$ and $KCaCl_3$ properties were calculated in Ref. [14]. Behavior of the $RbCaX_3$ ($X = F, Cl$) perovskites at ambient pressure was the subject of Ref. [15]. Finally, various approaches to study $CsCaF_3$ at ambient pressure were employed in Refs. [16–19]. It also can be noticed that the spectroscopic properties of various impurities in these perovskites were studied, e.g. Ni^{2+} [20] and Gd^{3+} [21] in $RbCaF_3$, V^{2+} [22] and Cr^{3+} [23] in $CsCaF_3$, Pr^{3+} and Ce^{3+} in $KCaF_3$ [24].

However, as far as the host's physical properties are concerned, no systematic comparison of all these properties across the series of these three compounds at the ambient and elevated pressure can be found. This has been done in the present paper. In addition, such parameters like Grüneisen constant and specific heat capacities were also calculated in this work. Besides, the elastic anisotropy of these crystals expressed in terms of directional dependence of the Young moduli (which also was analyzed in the present paper) has never been considered before. It should be also pointed out that very few experimental data for the considered perovskites exist in the literature.

The structure of the paper is as follows: the method and details of calculations are described in Section 2. All calculated results along with corresponding discussions are collected in Section 3 (which is divided into several subsections for easier reading). Section 4 contains the main conclusions of the presented calculations.

2. Method of calculations

All calculations were performed with the help of the CASTEP module [25] of Materials Studio package using either the generalized gradient approximation (GGA) with the Perdew-Burke-Ernzerhof functional [26] or the local density approximation (LDA) with the Ceperley-Alder-Perdew-Zunger (CA-PZ) functional [27,28]. The plane-wave basis energy cutoff was chosen to be 500 eV. The Monkhorst-Pack scheme k -points grid sampling was set at $10 \times 10 \times 10$ for the Brillouin zone. The convergence parameters were set as follows: total energy tolerance 5×10^{-6} eV atom⁻¹; maximum force tolerance 0.01 eV Å⁻¹; maximum stress 0.02 GPa; and maximum displacement 5×10^{-4} Å. The electronic configurations for all involved chemical elements were as follows: $5s^2 5p^6 6s^1$ for Cs, $4s^2 4p^6 5s^1$ for Rb, $3s^2 3p^6 4s^1$ for K, $3s^2 3p^6 4s^2$ for Ca and $2s^2 2p^5$ for F.

After the crystal structures were optimized with the above-given computational settings, the electronic, optical, elastic and

thermodynamic properties were calculated; all these results are presented below.

3. Results of calculations

3.1. Structural and electronic properties

All three perovskites considered in the present paper crystallize in the $Pm-3m$ space group (No. 221). There is one formula unit in a unit cell. The first and the second cations are 12- and 6-fold coordinated by the fluorine ions, respectively.

Table 1 contains a summary of the structural data for the three studied perovskites. As seen from the Table, the calculated lattice constants are highly consistent with the corresponding experimental results and with other theoretical data available in the literature. The lattice constants increase with increasing atomic number and ionic radii of the first cation (K – Rb – Cs).

It can be also noted that all the LDA-calculated lattice constants are somewhat smaller than their GGA counterparts. Correspondingly, the LDA-calculated densities and band gaps (also shown in Table 1) are greater in comparison with the GGA results. It should be noted that all calculated band gaps are underestimated in relation with the experimentally determined values. This is a common feature of the DFT-based calculations. Comparison of our calculated values with other theoretical data (except for those obtained by using the hybrid DFT approach [16]) yields good agreement and high consistency. In principle, the difference between the calculated and experimental band gaps can be overcome by using the scissor operator, which *a posteriori* shifts up the conduction band (CB) to make the calculated band gap be equal to the experimental value. In the present work we did not use such an operator and preferred to stay completely in the framework of the first-principles calculations without any empirical corrections.

The calculated band structures are shown in Fig. 1 in the same scale from -5 eV to 16 eV. For $KCaF_3$ and $RbCaF_3$ the band gaps are of indirect character: the CB minimum is realized at the G point (Brillouin zone center), whereas the maximum of the valence band (VB) is realized at the R point. The band gap of $CsCaF_3$ is direct. The value of the band gaps is increasing when going from K to Rb and Cs.

The electronic states at the VB top are remarkably flat, which indicates a low mobility of the holes. At the same time, the dispersion of the electronic states in the CB, and especially at its bottom, is quite strong and is especially pronounced in the vicinity of the G point.

If the CBs in all three perovskites are very similar, the VBs exhibit a clear difference: in $KCaF_3$ and $RbCaF_3$ they are very narrow (about 2 eV), whereas in $CsCaF_3$ the VB has a double structure: there is a narrow sub-band at about -4 eV separated by a gap of about 2 eV from the upper VB.

The origin of the calculated electronic band structure can be understood with the help of the partial density of states (PDOS) and total density of states (DOS) diagrams exhibited in Fig. 2. It is clear then that the CBs are dominated by the Ca 4s, 3d unoccupied states, together with the K 4s states in $KCaF_3$, Rb 5s states in $RbCaF_3$, and Cs 6s states in $CsCaF_3$.

The VBs between -2 eV and 0 eV are formed by the fluorine 2p states. The lower VB in $CsCaF_3$ between -5 eV and -4 eV (which is absent in $KCaF_3$ and $RbCaF_3$) consists of the Cs 5p states.

The Ca 3s and 3p states in all three considered materials form deep bands at about -36 eV and -16 eV. The s and p states of the first cation are gradually shifting up when moving from K to Rb and then to Cs. Thus, the 3s, 3p states of K are at about -26 eV and -10 eV, respectively, the 4s, 4p states of Rb are located at -23 eV and -7.5 eV, and, finally, the 5s, 5p states of Cs are peaked

Table 1A summary of the calculated and experimental structural and electronic properties of $X\text{CaF}_3$ ($X = \text{K}, \text{Rb}, \text{Cs}$) crystals.

		Lattice constant a (Å)	Volume V (Å ³)	Density ρ (kg m ⁻³)	Band gap E_g (eV)
KCaF ₃	Exp. ^a	4.4584	88.620	2551.516	6–13
	GGA ^b	4.4738	89.542	2525.274	6.169
	LDA ^b	4.3180	80.524	2808.584	6.313
	Calc. ^c	4.489	90.458	2498.881	6.14
RbCaF ₃	Exp. ^d	4.455	88.418	3428.202	10.9
	GGA ^b	4.5141	91.987	3295.308	6.403
	LDA ^b	4.3486	82.236	3686.049	6.629
	Calc. ^e	4.51	91.734	3303.231	6.39
CsCaF ₃	Exp. ^f	4.526	92.714	4117.658	–
	GGA ^b	4.5839	96.318	3963.585	6.893
	LDA ^b	4.4102	85.778	4450.612	7.272
	Calc. ^g	4.5691	95.388	4002.245	9.799

^a Refs. [29–31].^b This work.^c Ref. [14].^d Refs. [32,33].^e Ref. [15].^f Ref. [34].^g Ref. [16], hybrid DFT method.

at -17 eV and -5 eV (the latter ones approach the VB, as it was mentioned above).

The calculated effective Mulliken charges are presented in Table 2. As seen from Table 2, the effective charges of all ions differ considerably from the formal charges that can be expected from the chemical formulae. If the ionic charges of the K, Rb and Cs are close to their formal charges $+1$, the calculated charges of Ca in all three perovskites deviate from the formal value of $+2$. This shows that the first cations are bonded to the crystal lattice by the ionic bonds mainly, whereas the degree of covalency in the Ca – F bonds is much higher.

3.2. Optical properties

The knowledge of the electronic structure of a solid is the first step towards understanding of its optical properties. Fig. 3 shows the calculated absorption spectra of the three considered perovskites. The absorption starts in the region of the calculated band gap, the first absorption band is due to the transition from the 2p states of F in the VB to the lowest CB states (4s states of K, 5s states of Rb, 6s states of Cs in each particular case, and 3d states of Ca in all cases). The first absorption band is considerably wider in CsCaF₃, since the 5p states of Cs, closely located to the VB bottom, also

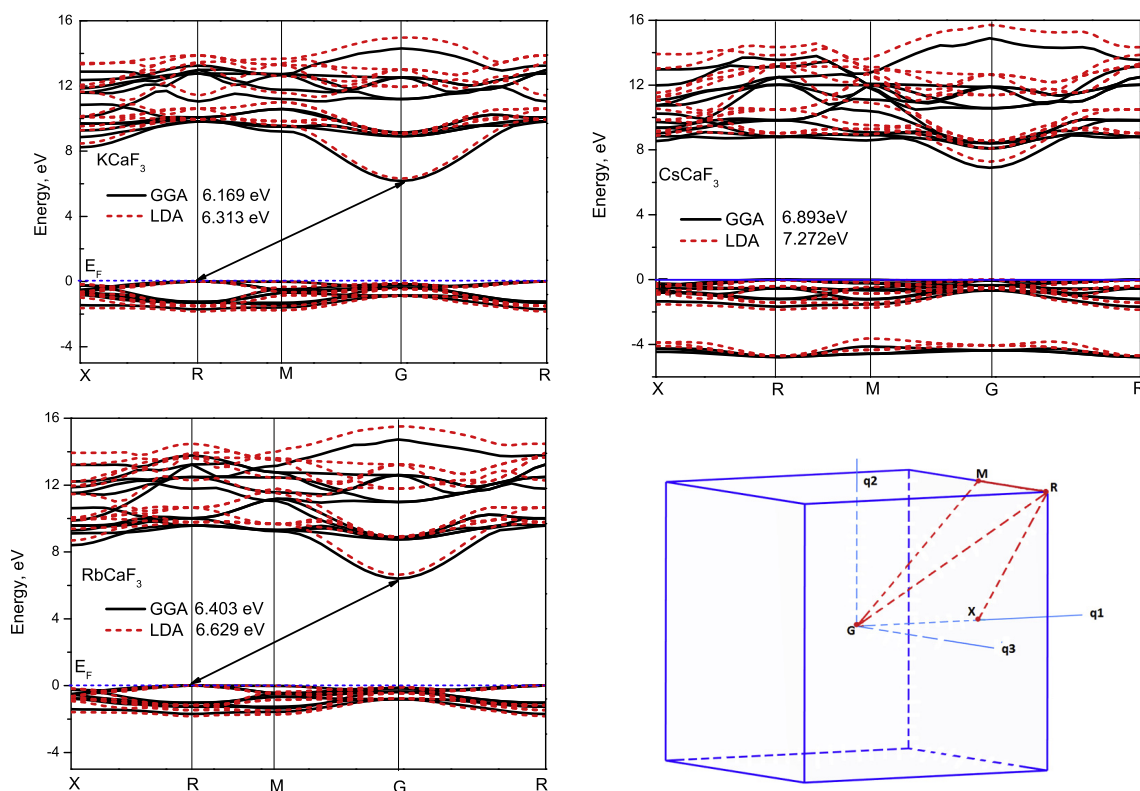


Fig. 1. The calculated band structures of $X\text{CaF}_3$ ($X = \text{K}, \text{Rb}, \text{Cs}$) crystals. The GGA- and LDA-calculated electronic bands are shown by the solid and dashed lines, respectively. The Fermi level is set at the VB top. The Brillouin zone (BZ) is also depicted; the path along which the electronic bands are shown in the figures of the band structures is highlighted.

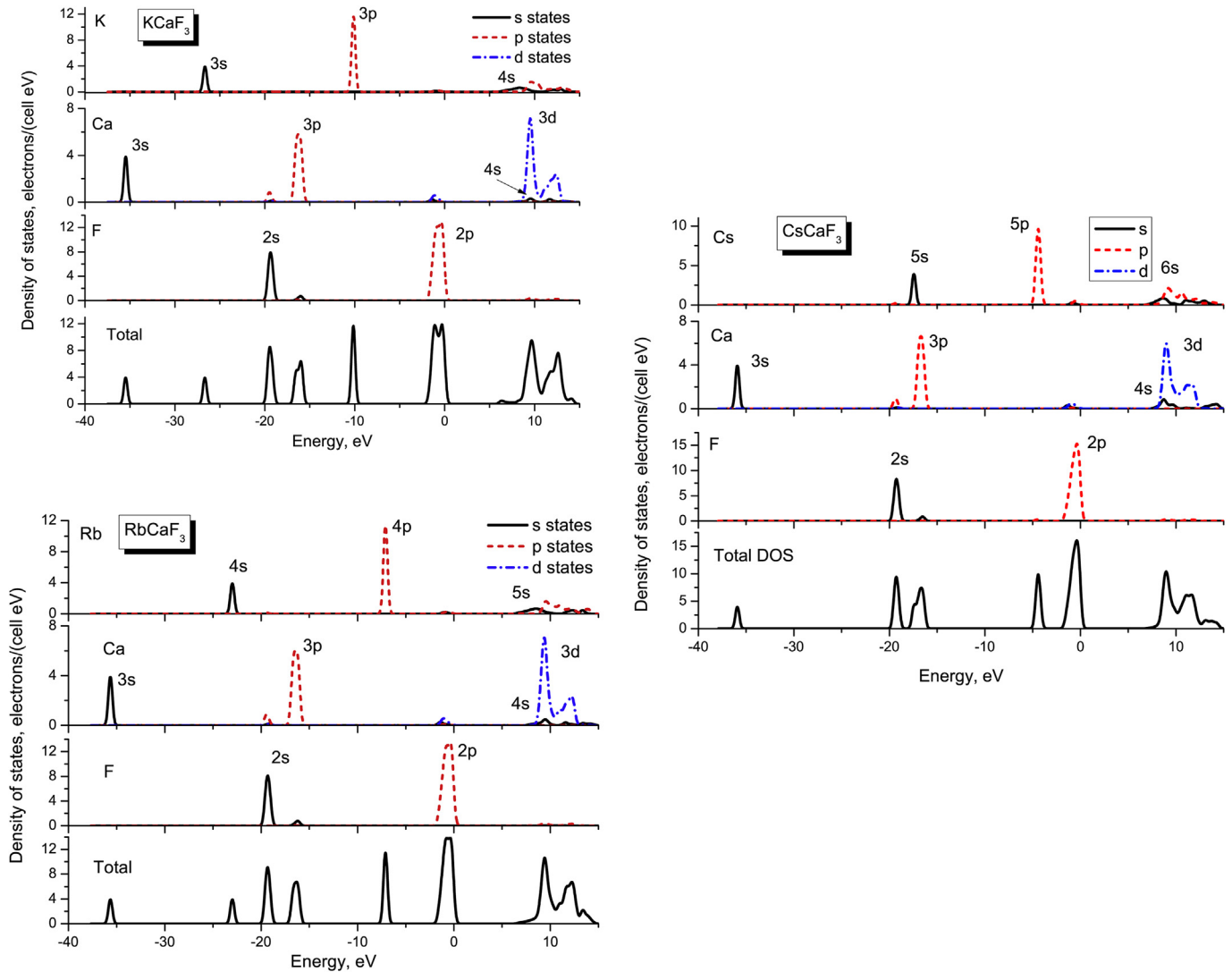


Fig. 2. The total and partial density of states (DOS) diagrams for $X\text{CaF}_3$ ($X = \text{K, Rb, Cs}$) crystals.

Table 2

Calculated atomic populations and effective Mulliken charges (in units of the proton's charge) for $X\text{CaF}_3$ ($X = \text{K, Rb, Cs}$) crystals (GGA/LDA values).

Crystal	Ion	s-electrons	p-electrons	d-electrons	Total	Charge
KCaF ₃	K	2.10/2.12	6.07/6.04	0.00/0.00	8.17/8.15	0.83/0.85
	Ca	2.24/2.27	6.00/6.00	0.55/0.64	8.80/8.91	1.20/1.09
	F	1.96/1.96	5.72/5.69	0.00/0.00	7.68/7.65	-0.68/-0.65
RbCaF ₃	Rb	2.12/2.13	6.05/6.02	0.00/0.00	8.17/8.15	0.83/0.85
	Ca	2.26/2.28	6.00/6.00	0.54/0.62	8.80/8.91	1.20/1.09
	F	1.96/1.96	5.72/5.69	0.00/0.00	7.68/7.65	-0.68/-0.65
CsCaF ₃	Cs	2.14/2.13	6.01/5.99	0.00/0.00	8.15/8.12	0.85/0.88
	Ca	2.27/2.30	6.00/6.00	0.51/0.60	8.79/8.89	1.21/1.11
	F	1.96/1.96	5.73/5.70	0.00/0.00	7.69/7.66	-0.69/-0.66

contribute to the absorption between 15 and 20 eV. The intensity of the first absorption band is higher in the case of the LDA calculations, which correlates with smaller lattice constants calculated by LDA (Table 1), decreased interionic separations (compared with the GGA corresponding results) and, as a consequence, increased overlap of the fluorine and metal ions orbitals.

Assignment of the remaining bands can be done as follows. A weaker structured absorption band between 15 eV and 25 eV in

KCaF₃ is due to the transitions from the 3p states of Ca and K to the CB states. Finally, two sharp maxima at about 26 eV and 28 eV arise from the transitions from the F 2s states to the CB.

In RbCaF₃ the band between 15 eV and 22 eV is formed by the transitions from the Rb 4p, Ca 3p states to the CB, and absorption from the 3p states of Ca together with the 2s states of F produces sharp peaks at higher energy of 26 eV and 28 eV; these bands in CsCaF₃ have the same origin.

The calculated real and imaginary parts of the dielectric function for all three perovskites are shown in Fig. 4. The imaginary part $\text{Im}(\epsilon)$ is proportional to the absorption spectrum of a solid; all main peaks in the $\text{Im}(\epsilon)$ curves in Fig. 4 coincide with the absorption spectra features in Fig. 3. It can be also noted that $\text{Im}(\epsilon)$ is always positive in KCaF₃ and RbCaF₃. However, for CsCaF₃ $\text{Im}(\epsilon)$ becomes negative at about -14 eV. The real part $\text{Re}(\epsilon)$ describes the dispersion properties of a solid. The square root of $\text{Im}(\epsilon)$ in the limit of infinitely long wavelengths determines the value of the refractive index of a medium, which – in the case of the considered perovskites is in the range of 1.3–1.4. These estimations agree with the corresponding experimental values of the refractive index of 1.39 for KCaF₃ [35] and theoretical estimations of 1.53 for CsCaF₃ [18] and 1.46 for RbCaF₃ [36].

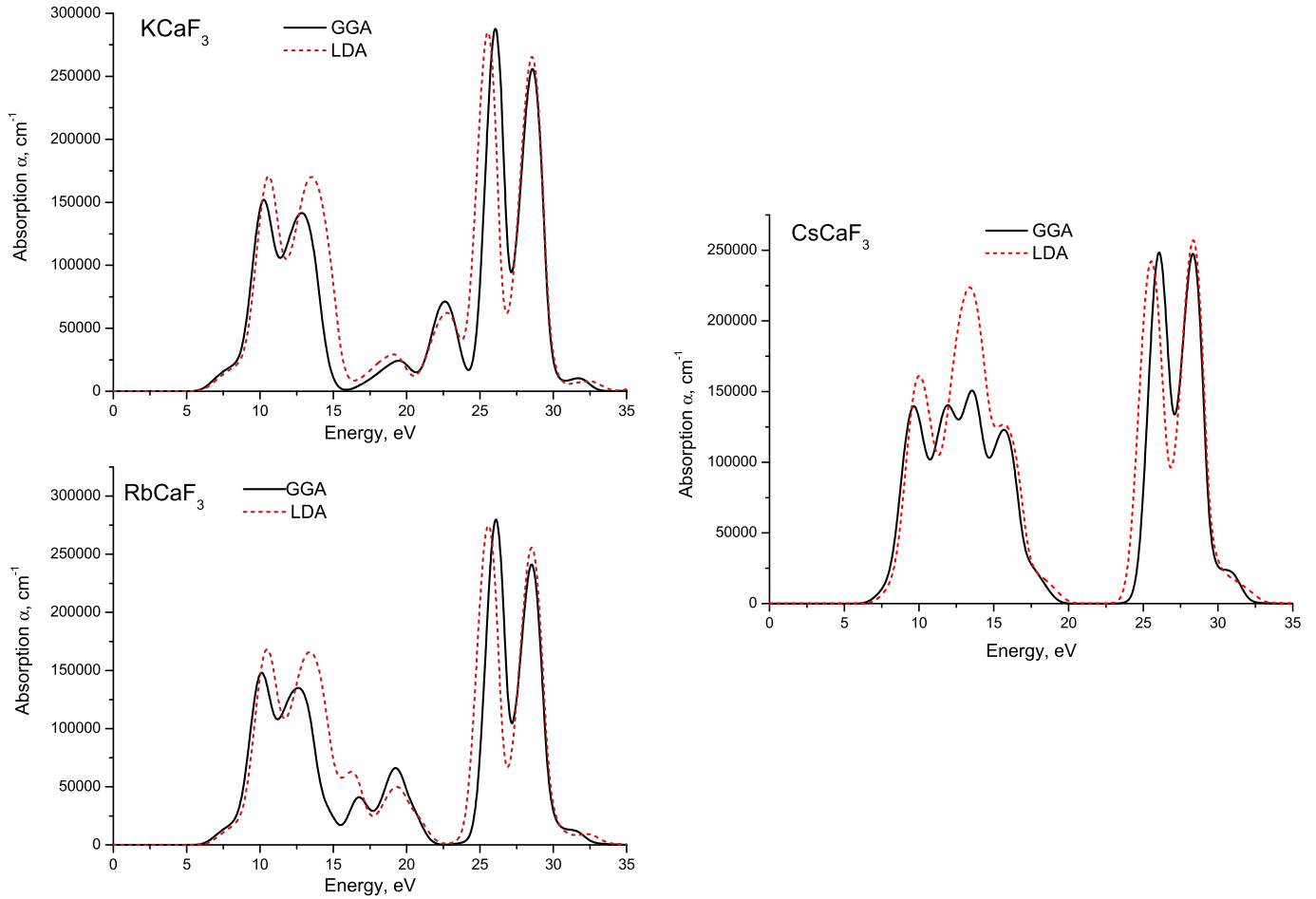


Fig. 3. Calculated absorption spectra of $XCaF_3$ ($X = K, Rb, Cs$) crystals.

3.3. Elastic and thermodynamic properties

Only three elastic constants C_{11} , C_{12} , C_{44} are needed to describe completely the elastic properties of cubic crystals. These constants have been calculated in both GGA and LDA runs, with the computational settings described above. Table 3 below gives a summary of the calculated results, in comparison with the available experimental and/or theoretical data found in other publications.

After the elastic constants are calculated, one can estimate the sound velocities in a solid and its Debye temperature Θ_D , related to the maximum phonon energy in the Debye model, using the following equation [38].

$$\Theta_D = \frac{h}{k} \left[\frac{3n}{4\pi} \left(\frac{N_A \rho}{M} \right) \right]^{1/3} v_m \quad (1)$$

where h and k are the Planck's and Boltzmann's constants, respectively, N_A is the Avogadro's number, ρ is the crystal's density, M is the molecular weight, n denotes the number of atoms per one formula unit (five for all considered materials), v_m is the mean sound velocity expressed in terms of the longitudinal v_l and

transverse v_t sound velocities as $v_m = \left[\frac{1}{3} \left(\frac{2}{v_t^3} + \frac{1}{v_l^3} \right) \right]^{-1/3}$ [39] and

$v_l = \sqrt{\frac{3B+4G}{3\rho}}$, $v_t = \sqrt{\frac{G}{\rho}}$ [40] with B being the bulk modulus and $G = \frac{C_{11}+C_{12}}{2}$ the isotropic shear modulus estimated as the average

value of the Voigt's shear modulus G_V (an upper limit for G values) and Reuss's shear modulus G_R (a lower limit for G values), calculated using the elastic constants C_{ij} : $G_V = \frac{C_{11}-C_{12}+3C_{44}}{5}$, $\frac{5}{G_R} = \frac{4}{C_{11}-C_{12}} + \frac{3}{C_{44}}$ [40].

The calculated values of the sound velocities, Debye temperatures and Grüneisen constants (its definition and method of calculations will be given later on, when the pressure effects will be described) are collected in Table 4.

There is a monotonic decrease in the sound velocities with increased atomic number of the first cation; as a consequence, the calculated Debye temperature is also decreased. On the contrary, the Grüneisen constants increase in the same direction, which suggests a stronger dependence of the phonon frequencies on a unit cell volume (or, eventually, on pressure).

With the obtained values of the Debye temperature it is also possible to calculate the phonon contribution to the specific heat capacity C_V^{ph} as [42].

$$C_V^{ph} = 9knN_A \left(\frac{T}{\Theta_D} \right)^3 \int_0^{\Theta_D/T} \frac{x^4 \exp(x)}{(\exp(x) - 1)^2} dx, \quad (2)$$

where n denotes the number of atoms in a chemical formula and T is the absolute temperature.

The results of the calculated specific heat capacities are shown in Fig. 5. Already at the room temperatures the molar heat

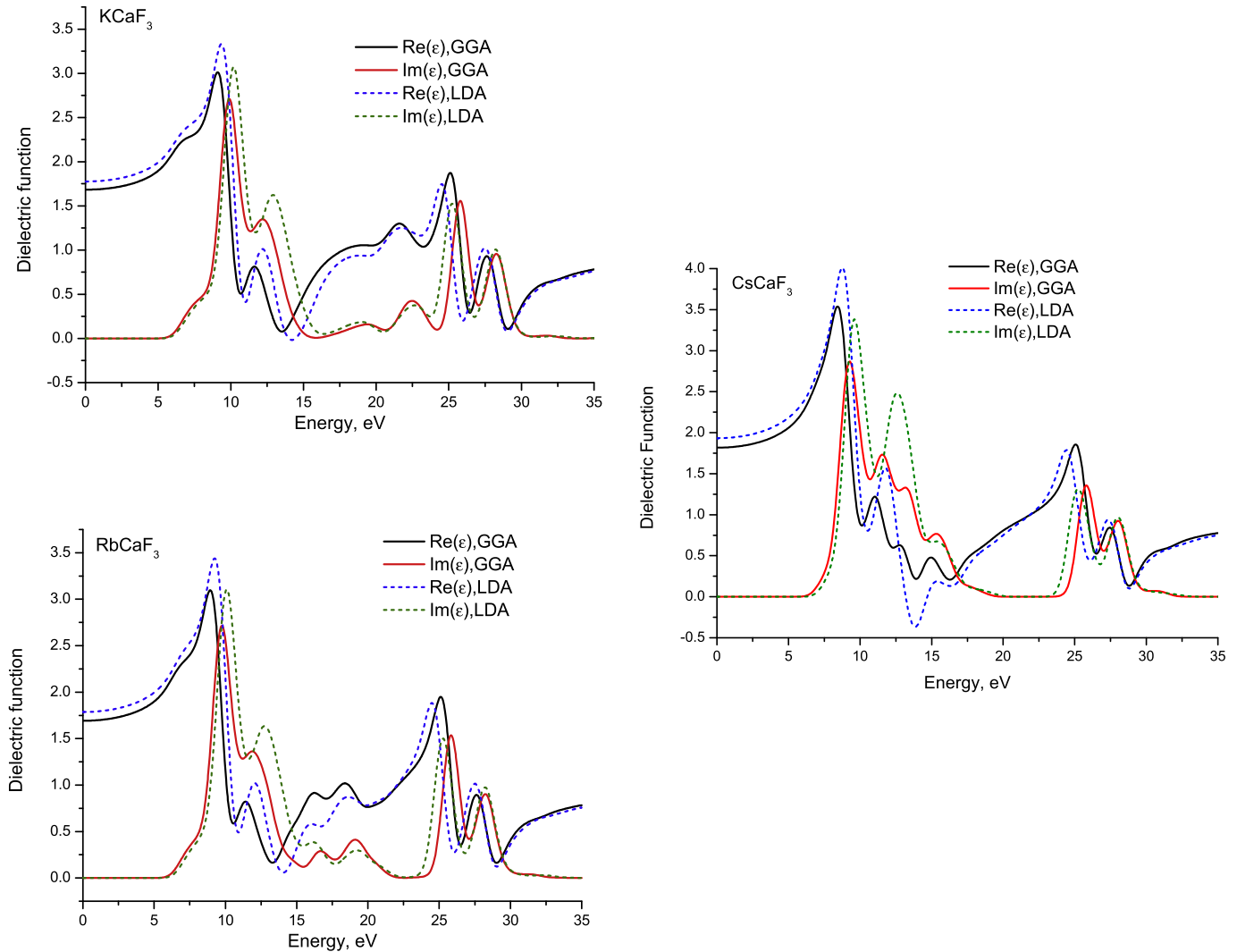


Fig. 4. The real and imaginary parts of dielectric function ϵ calculated by GGA and LDA as a function of photon energy for XCaF_3 ($X = \text{K, Rb, Cs}$) crystals.

Table 3

Elastic constants C_{11} , C_{12} , C_{44} , bulk B and Young E moduli (all in GPa) and non-dimensional Poisson ratio γ for XCaF_3 ($X = \text{K, Rb, Cs}$) crystals.

		C_{11}	C_{12}	C_{44}	B	E	γ
KCaF ₃	GGA ^a	109.40	22.25	16.84	51.30	101.89	0.169
	LDA ^a	146.45	19.84	15.68	62.04	141.71	0.119
	Calc. ^b	103.0	18.0	16.0	46.0	61.3	0.280
RbCaF ₃	GGA ^a	99.46	20.36	19.66	46.72	92.54	0.170
	LDA ^a	141.76	23.55	19.69	62.96	135.05	0.143
	Calc. ^c	82.23	12.56	16.20	35.78	55.05	0.243
CsCaF ₃	GGA ^a	90.26	24.39	23.04	46.34	79.88	0.200
	LDA ^a	133.32	32.20	25.19	65.91	120.80	0.195
	Calc. ^d	98.46	24.81	27.64	49.36	—	—
	Exp. ^e	102.0	25.3	25.5	50.87	—	—

^a Calc. (present work).

^b Calc. (Ref. [11]).

^c Calc. (Ref. [15]).

^d Calc. (Ref. [16]).

^e Exp. (Ref. [37]).

Table 4

Longitudinal v_l , transverse v_t and mean v_m sound velocities (all in m/s), Debye temperature Θ_D (K), and non-dimensional Grüneisen constant γ_G for XCaF_3 ($X = \text{K, Rb, Cs}$) crystals.

		v_l	v_t	v_m	Θ_D	γ_G
KCaF ₃	GGA ^a	5754	3141	3503	399	0.931
	LDA ^a	5987	3191	3565	420	0.833
	Calc. ^b	6419	2530	2867	392	—
RbCaF ₃	GGA ^a	4954	2816	3131	353	1.187
	LDA ^a	5337	2909	3245	380	1.123
	Calc. ^c	4448	2590	2873	324	—
CsCaF ₃	GGA ^a	4543	2590	2879	320	1.481
	LDA ^a	4982	2741	3055	353	1.398
	Calc. ^d	4736	2717	3018	342	—

^a Calc. (present work).

^b Calc. (Ref. [11]).

^c Calc. (Ref. [15]).

^d Calc. (Ref. [41]).

capacities for all studied perovskites approach the limiting value of about 124 J/(mol K), which is in agreement with the Petit and Dulong law for the solids with 5 atoms in a chemical formula. Since the calculated Debye temperatures for RbCaF₃ (GGA) and CsCaF₃

(LDA) are accidentally the same, the corresponding lines in Fig. 5 coincide with each other. It is also seen from Fig. 5 that the specific heat capacities are increasing when going from K to Rb and Cs, if the temperature is kept fixed.

Although the considered crystals have the cubic structure, they,

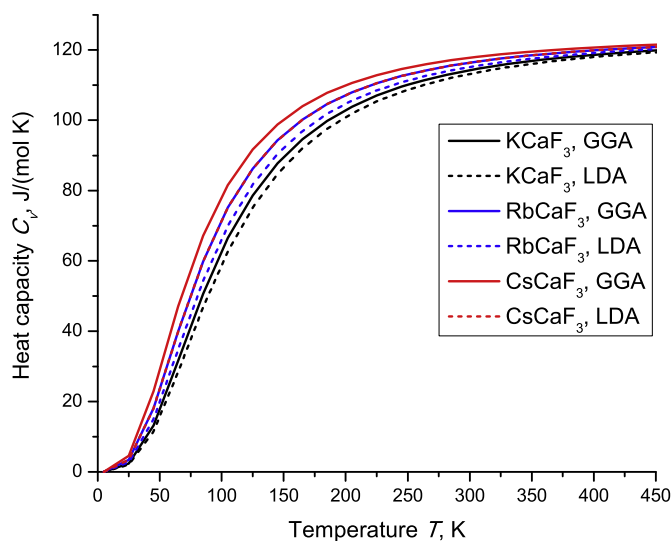


Fig. 5. Calculated phonon contributions to the specific heat capacity for $X\text{CaF}_3$ ($X = \text{K}, \text{Rb}, \text{Cs}$) crystals.

nevertheless, possess certain elastic anisotropy: response of the crystal lattice to the deformations applied along the (100), (110) and (111) directions will be, of course, different. Such anisotropy can be analyzed with the help of the directional dependence of the Young modulus E , which in the case of a cubic crystal is described by the following equation [43]:

$$E(\vec{n}) = \frac{1}{S_{11} - \beta_1(n_1^2n_2^2 + n_1^2n_3^2 + n_2^2n_3^2)}, \text{ where } \beta_1 = 2S_{11} - 2S_{12} - S_{14} \quad (3)$$

The S_{ij} symbol in Eq. (3) denotes the elastic compliance constants, which form the matrix inverse to the matrix of the elastic constants C_{ij} , and n_1, n_2, n_3 are the direction cosines, which determine the direction in the crystal lattice. For a perfect elastically isotropic medium the surface given by Eq. (3) would be a sphere. However, this is not the case with the considered in the present paper cubic perovskite crystals. As Fig. 6 shows, the shapes of all three surfaces differ from the ideal spherical shape. The maximal values of the Young moduli are realized along the a, b and c axes (i.e. (100), (010), (001) directions). The corresponding numerical values (all in GPa, GGA/LDA data) are as follows: $\text{KCaF}_3 - 101.89/141.70$, $\text{RbCaF}_3 - 92.54/135.05$, $\text{CsCaF}_3 - 79.88/120.79$, whereas the smallest Young moduli are along the (111) direction with the following values (the same notation as above): $\text{KCaF}_3 - 45.55/43.39$, $\text{RbCaF}_3 - 51.74/53.49$, and $\text{CsCaF}_3 - 59.29/67.03$. The difference between the maximal and minimal Young values can be quite significant and they can differ by a factor of more than 2.

3.4. Pressure effects

Application of hydrostatic pressure to a solid with the cubic crystal structure will lead to a uniform compression of its crystal lattice. Since the interionic distances in a solid will be changed with pressure, its physical properties such as electronic, optical, elastic etc, will be changed as well.

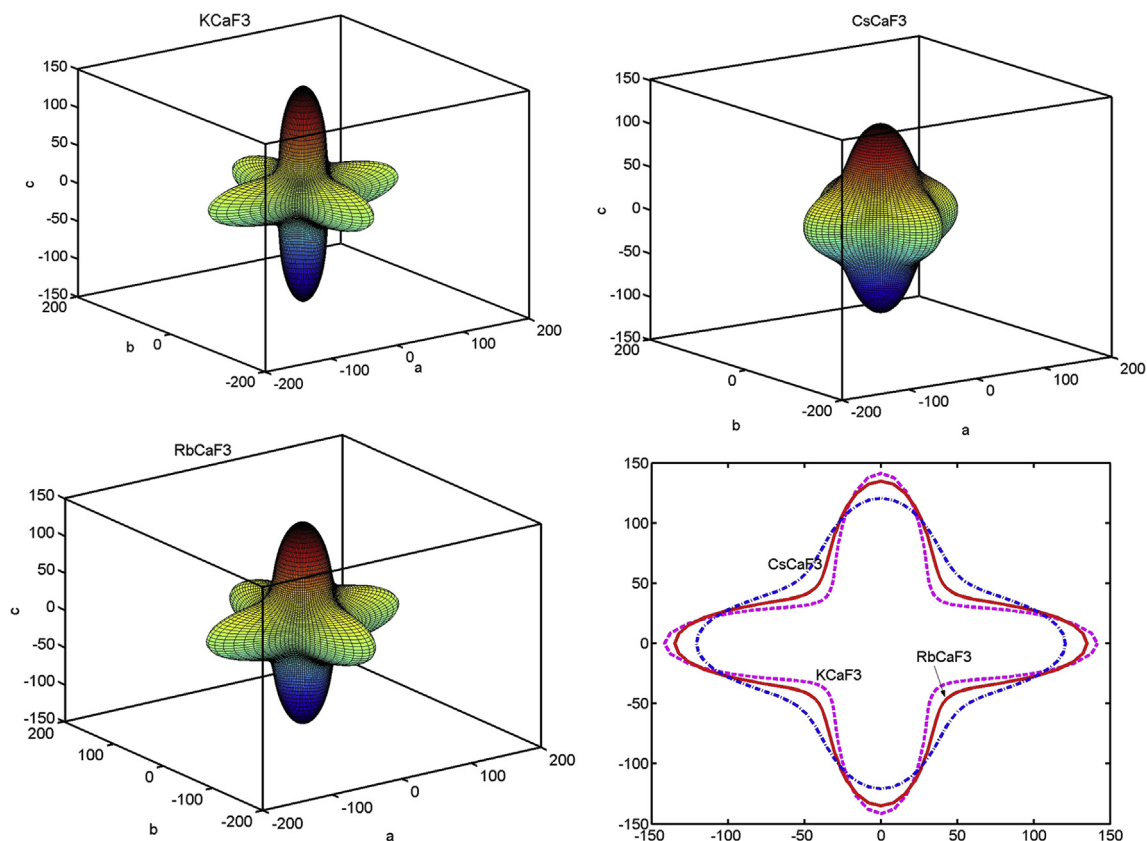


Fig. 6. Three-dimensional dependences of the calculated Young moduli (LDA results) and their cross-sections for $X\text{CaF}_3$ ($X = \text{K}, \text{Rb}, \text{Cs}$) crystals. The axes units are GPa.

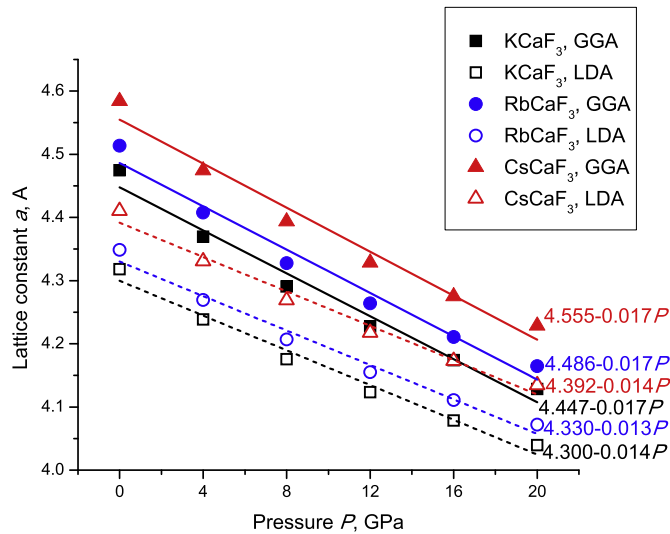


Fig. 7. Calculated lattice constants (symbols) and their linear approximations as functions of pressure P (lines) for $XCaF_3$ ($X = K, Rb, Cs$) crystals. The equations of linear fits are also shown.

To model the pressure effects on the properties of the studied perovskites, their crystal structures were optimized at the ambient and elevated hydrostatic pressures of 4, 8, 12, 16 and 20 GPa. All calculating settings were the same as those given when describing the details of calculations.

Fig. 7 shows dependence of the calculated lattice constants on pressure. As seen from the Figure, the calculated data follow the linear dependence on pressure. Equations of the linear fits of the calculated data points are also given in the Figure. All calculated lattice constants exhibit a similar rate of variation with pressure from -0.013 to -0.017 Å/GPa.

The next step in the analysis of the pressure effects is the application of the Murnaghan equation of state [44]:

$$\frac{V}{V_0} = \left(1 + B'_0 \frac{P}{B_0}\right)^{-1/B'_0}, \quad (4)$$

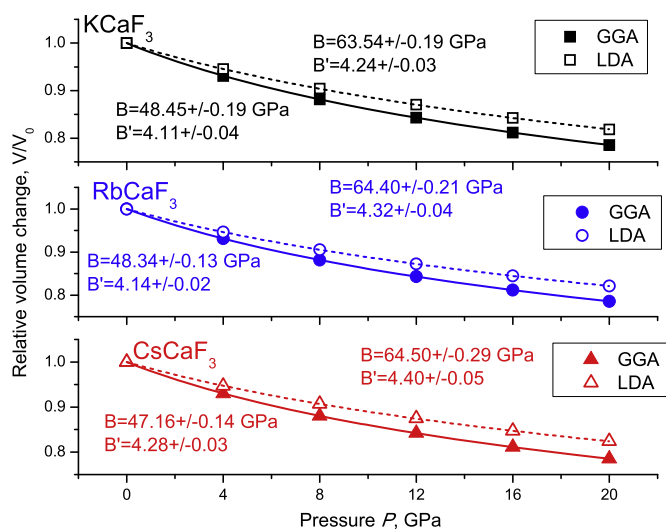


Fig. 8. Calculated relative changes of the unit cell volumes (symbols) and their fits to the Murnaghan equation of states (lines) at different values of hydrostatic pressure P for $XCaF_3$ ($X = K, Rb, Cs$) crystals.

where V and V_0 are the unit cell volume at the pressure P and ambient pressure, respectively, B_0 is the bulk modulus at the ambient pressure, and B'_0 is its pressure derivative. The results of application of Eq. (4) to the calculated variation of the unit cell volume with pressure are shown in Fig. 8, along with the extracted from the fit values of B_0 and B'_0 . The LDA-calculated data show somewhat smaller compressibility than the GGA ones. The value of the bulk modulus pressure derivatives for all cases is in the range from 4.1 to 4.4, which is typical for solids.

Band gaps of these perovskites increase with pressure, as illustrated by Fig. 9 (the GGA and LDA results are shown in different figures, to avoid data point overlapping). The dependence of the calculated band gaps (shown by different symbols) on pressure can be fitted by the linear functions. In the case of CsCaF₃ the band gap bowing effects (for the LDA calculated data) are more pronounced.

Behavior of the elastic constants C_{ij} with pressure is depicted in Fig. 10. All elastic constants are perfect linear functions of applied pressure P . The equations of linear approximations of the calculated values are collected in Table 5. It can be noted that the slopes of the linear fits in both GGA and LDA results are close for each elastic constant – the corresponding lines are practically parallel to each other. Moreover, the slopes of the bulk modulus dependences on

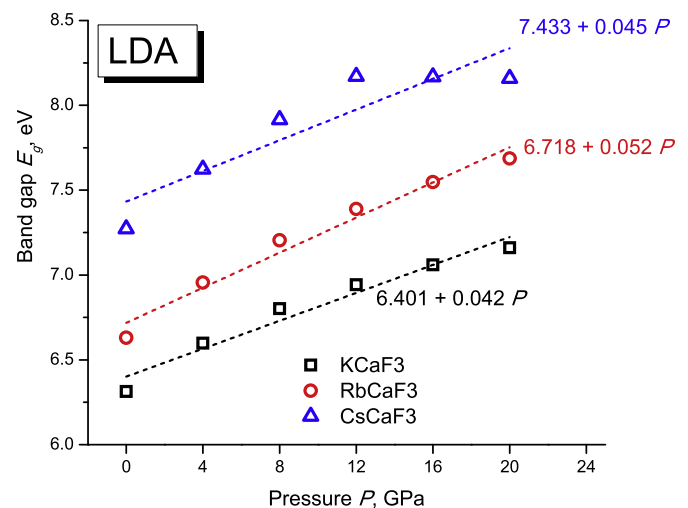
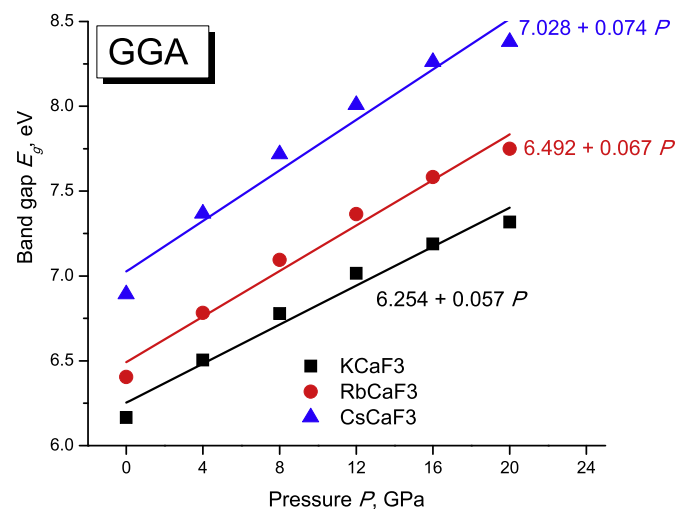


Fig. 9. Calculated values of the band gaps E_g (symbols) and their linear fits (lines) at different values of hydrostatic pressure P for $XCaF_3$ ($X = K, Rb, Cs$) crystals. Equations of fits are also given.

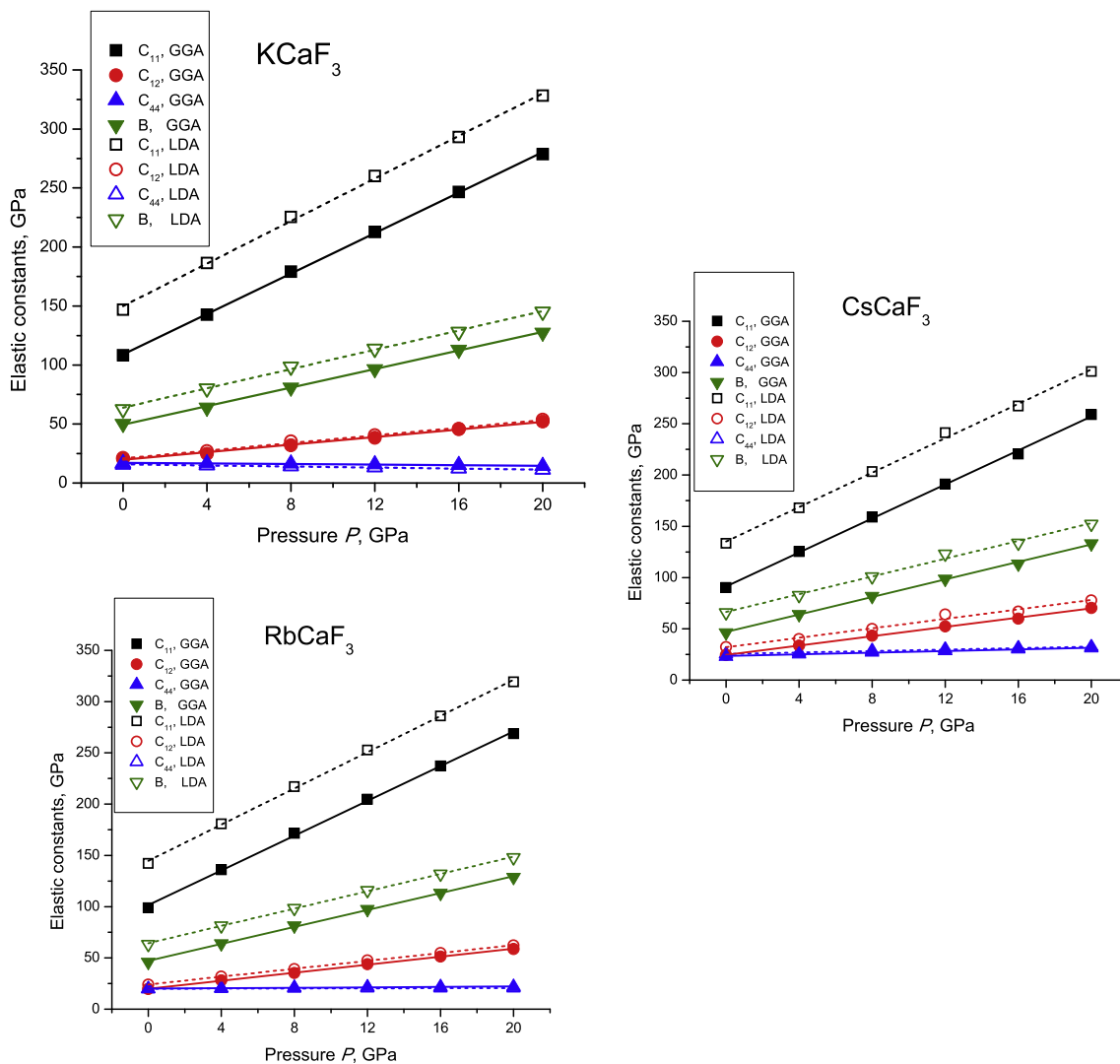


Fig. 10. Calculated values of the elastic constants (symbols) and their linear fits (lines) of hydrostatic pressure P for $X\text{CaF}_3$ ($X = \text{K}, \text{Rb}, \text{Cs}$) crystals.

Table 5

Linear approximations of the elastic constants as functions of pressure P for $X\text{CaF}_3$ ($X = \text{K}, \text{Rb}, \text{Cs}$) crystals.

		C_{11}	C_{12}	C_{44}	B
KCaF ₃	GGA	$109.07 + 8.56P$	$19.80 + 1.60P$	$17.14 - 0.13P$	$49.55 + 3.92P$
	LDA	$149.98 + 9.01P$	$20.83 + 1.63P$	$15.84 - 0.22P$	$63.88 + 4.09P$
RbCaF ₃	GGA	$101.40 + 8.48P$	$19.94 + 1.95P$	$19.99 + 0.11P$	$47.25 + 4.12P$
	LDA	$144.73 + 8.83P$	$24.07 + 1.92P$	$19.90 + 0.03P$	$64.29 + 4.22P$
CsCaF ₃	GGA	$91.27 + 8.30P$	$24.65 + 2.27P$	$23.50 + 0.40P$	$46.86 + 4.28P$
	LDA	$135.18 + 8.39P$	$32.06 + 2.30P$	$25.49 + 0.35P$	$66.44 + 4.33P$

pressure are close to the B' values determined from the Murnaghan equation.

Finally, the calculations of the equilibrium lattice constants and elastic constants at elevated hydrostatic pressures can help in estimating the Grüneisen constant γ_G , which shows how the phonon frequencies (and, eventually, Debye temperature Θ_D) vary with the volume V of the crystal. The following equation can be used for this purpose [45]:

$$\gamma_G = -\frac{d \ln \Theta_D}{d \ln V} = -\frac{V}{\Theta_D} \frac{d \Theta_D}{d V}. \quad (5)$$

Knowledge of the optimized lattice constants and elastic constants at various pressures allows to calculate the Debye temperature and, eventually, the slope $\frac{d \Theta_D}{d V}$ (Fig. 11). The calculated values of γ_G are shown in Table 4. It is seen that its values increase when going from the lighter cation K to the heavier ones Rb and Cs.

4. Conclusions

Detailed ab initio calculations of the structural, electronic, optical, elastic and thermodynamic properties of three fluoroperovskites $X\text{CaF}_3$ ($X = \text{K}, \text{Rb}, \text{Cs}$) have been performed in the present paper. The structures of these compounds were optimized at the

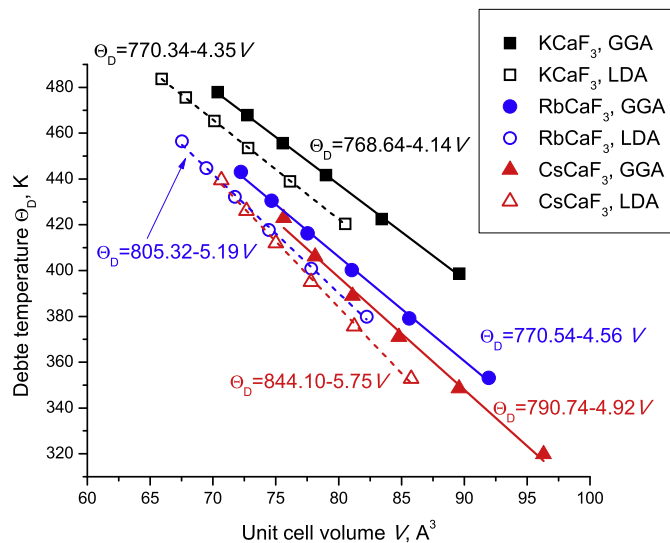


Fig. 11. Calculated dependence of the Debye temperature Θ_D (symbols) on the unit cell V and the linear fits (lines) for $X\text{CaF}_3$ ($X = \text{K}, \text{Rb}, \text{Cs}$) crystals. Equations of linear fits are also given.

ambient and elevated hydrostatic pressure, in the pressure range from 0 to 20 GPa. The electronic, elastic, thermodynamic properties were calculated and compared, whenever possible, to the experimental data; their dependences on pressure was modeled and represented by the linear (lattice and elastic constants) and parabolic (band gaps) functions of pressure. The elastic anisotropy (dependence of the Young moduli on the direction in the crystal lattice) was visualized. The changes of all these properties with varying the first cation (K – Rb – Cs) were followed.

Acknowledgements

The project was funded by National Natural Science Foundation of China (11404047), Chongqing Research Program of Basic Research and Frontier Technology (No. CSTC2014JCYJA50034), and Research Training Program for Undergraduates of Chongqing University of Posts and Telecommunications (Grant No. A2015-86). M.G. Brik thanks the supports from the Recruitment Program of High-end Foreign Experts (Grant No. GDW20145200225), the Programme for the Foreign Experts offered by Chongqing University of Posts and Telecommunications, Ministry of Education and Research of Estonia, Project PUT430, and European Regional Development Fund (TK141). A.H. Reshak would like to acknowledge the CENTEM project, reg. no. CZ.1.05/2.1.00/03.0088, co-funded by the ERDF as part of the Ministry of Education, Youth and Sports OP RDI program and, in the follow-up sustainability stage, CENTEM PLUS (LO1402) by financial means from the Ministry of Education, Youth and Sports under the "National Sustainability Programme I", the MetaCentrum (LM2010005) and CERIT-SC (CZ.1.05/3.2.00/

08.0144) infrastructures. The calculations have been carried out using resources provided by Wrocław centre for Networking and Supercomputing (<http://wcss.pl>), grant No. WCSS#10117290).

References

- [1] L.Q. Jiang, J.K. Guo, H.B. Liu, M. Zhu, X. Zhou, P. Wu, C.H. Li, J. Phys. Chem. Solids 67 (2006) 1531.
- [2] R.L. Moreira, A. Dias, J. Phys. Chem. Solids 68 (2007) 1617.
- [3] A.S. Verna, V.K. Jindal, J. Alloys Compd. 485 (2009) 514.
- [4] V. Luana, A. Costales, A. Martín Pendás, Phys. Rev. B 55 (1997) 4285.
- [5] V.V. Lemanov, A.V. Sotnikov, E.P. Smirnova, M. Weihnacht, R. Kunze, Solid State Commun. 110 (1999) 611.
- [6] U. Brauch, U. Dürr, Opt. Commun. 55 (1985) 35.
- [7] R.E. Cohen, Nature 358 (1992) 136.
- [8] K.D. Kreuer, Solid State Ionics 125 (1999) 285.
- [9] X. Liu, K. Sohlberg, Complex Metals Open Access J. 1 (2014) 103.
- [10] G. Murtaza, I. Ahmad, A. Afaq, Solid State Sci. 16 (2013) 152.
- [11] Sh Soleimanpour, F. Kanjouri, Ind. J. Phys. 89 (2015) 687.
- [12] B. Ghebouli, M. Fatmi, M.A. Ghebouli, H. Choutri, L. Louail, T. Chihi, A. Bouhemadou, S. Bin-Omran, Solid State Sci. 43 (2015) 9.
- [13] K.E. Babu, N. Murali, K.V. Babu, B.K. Babu, V. Veeraiyah, in: AIP Conf. Proc. 1661, 2015, p. 100002.
- [14] A.A. Mousa, Int. J. Mod. Phys. B 28 (2014) 1450139.
- [15] A.A. Mubarak, Int. J. Mod. Phys. B 28 (2014) 1450192.
- [16] C.-G. Ma, M.G. Brik, Comput. Mater. Sci. 58 (2012) 101.
- [17] A. Meziani, H. Belkhir, Comput. Mater. Sci. 61 (2012) 67.
- [18] K.E. Babu, A. Veeraiyah, D.T. Swamy, V. Veeraiyah, Chin. Phys. Lett. 29 (2012) 117102.
- [19] G. Vaitheeswaran, V. Kanchana, X.X. Zhang, Y.M. Ma, A. Svane, N.E. Christensen, J. Phys. Condens. Matter 28 (2016) 315403.
- [20] B. Villacampa, R. Alcalá, P.J. Alonso, J.M. Spaeth, J. Phys. Condens. Matter 5 (1993) 747.
- [21] H. Takeuchi, H. Ebisu, M. Arakawa, J. Phys. Condens. Matter 7 (1995) 1417.
- [22] Y. Qiu, J. Phys. Condens. Matter 3 (1991) 4877.
- [23] S. Lopez-Moraza, L. Seijo, Z. Barandiaran, Int. J. Quant. Chem. 77 (2000) 961.
- [24] Z. Mazurak, A. Ratuszna, P. Daniel, J. Lumin. 82 (1999) 163.
- [25] S.J. Clark, M.D. Segall, C.J. Pickard, P.J. Hasnip, M.J. Probert, K. Refson, M.C. Payne, Z. Krist. 220 (2005) 567.
- [26] J.P. Perdew, K. Burke, M. Ernzerhof, Phys. Rev. Lett. 77 (1996) 3865.
- [27] D.M. Ceperley, B.J. Alder, Phys. Rev. Lett. 45 (1980) 566.
- [28] J.P. Perdew, A. Zunger, Phys. Rev. B 23 (1981) 5048.
- [29] D.Z. Demetriou, C.R.A. Catlow, A.V. Chadwick, G.J. McIntyre, I. Abrahams, Solid State Ionics 176 (2005) 1571.
- [30] P.H. Daniel, M. Rousseau, J. Toulouse, Phys. Stat. Solidi (b) 203 (1997) 327.
- [31] J.W. Flocken, R.A. Guenther, J.R. Hardy, L.L. Boyer, Phys. Rev. Lett. 56 (1986) 1738.
- [32] A. Bulou, C. Ridou, M. Rousseau, J. Nouet, A. Hewat, J. Phys. C 17 (1984) 87.
- [33] A.N. Belsky, P. Chevallier, E.N. Melchakov, C. Pedrini, P.A. Rodnyi, A.N. Vasilev, Chem. Phys. Lett. 278 (1997) 369.
- [34] C. Ridou, M. Rousseau, J. Bouillot, C. Vettier, J. Phys. C 17 (1984) 1001.
- [35] C. Ambrosch-Draxl, J.O. Sofo, Comput. Phys. Commun. 175 (2006) 1.
- [36] A.A. Mousa, J.M. Khalifeh, N.T. Mahmoud, H.K. Juwhari, Am. J. Condens. Phys. 3 (2013) 151.
- [37] C. Ridou, M. Rousseau, F. Gervais, J. Phys. C 19 (1986) 5757.
- [38] O.L. Anderson, J. Phys. Chem. Solids 24 (1963) 909.
- [39] J.-P. Poirier, Introduction to the Physics of the Earth's Interior, Cambridge University Press, 2000.
- [40] E. Schreiber, O.L. Anderson, N. Soga, Elastic Constants and Their Measurements, McGraw-Hill, New York, 1973.
- [41] B. Salmankurt, S. Duman, Mater. Res. Express 3 (2016) 045903.
- [42] N.W. Ashcroft, N.D. Mermin, Solid State Physics, Holt, Rinehart and Winston, New York, 1976.
- [43] A. Cazzani, M. Rovati, Int. J. Solids Struct 40 (2003) 1713.
- [44] F.D. Murnaghan, Proc. Natl. Acad. Sci. 30 (1944) 244.
- [45] R. Hill, Proc. Phys. Soc. A 65 (1952) 349.